

A Presynaptic Role for the Cytomatrix Protein GIT in Synaptic Vesicle Recycling

Jasmin Podufall,^{1,4} Rui Tian,^{2,5} Elena Knoche,³ Dmytro Puchkov,^{1,4} Alexander M. Walter,^{1,2,3} Stefanie Rosa,^{1,2} Christine Quentin,² Anela Vukoja,^{1,4} Nadja Jung,⁴ Andre Lampe,^{1,4} Carolin Wichmann,² Mathias Böhme,² Harald Depner,² Yong Q. Zhang,⁵ Jan Schmoranzler,^{1,4} Stephan J. Sigrist,^{2,3,*} and Volker Haucke^{1,3,4,*}

¹Leibniz Institute for Molecular Pharmacology, Robert Rössle Strasse 10, 13125 Berlin, Germany

²Genetics, Institute for Biology, Freie Universität Berlin, Takustraße 6, 14195 Berlin, Germany

³NeuroCure Cluster of Excellence, Charité Universitätsmedizin Berlin, Virchowweg 6, 10117 Berlin, Germany

⁴Membrane Biochemistry, Institute of Chemistry & Biochemistry, Freie Universität Berlin, Takustraße 6, 14195 Berlin, Germany

⁵Institute of Genetics and Developmental Biology, Chinese Academy of Sciences, Beijing 100101, China

*Correspondence: stephan.sigrist@fu-berlin.de (S.J.S.), haucke@fmp-berlin.de (V.H.)

<http://dx.doi.org/10.1016/j.celrep.2014.04.051>

This is an open access article under the CC BY-NC-ND license (<http://creativecommons.org/licenses/by-nc-nd/3.0/>).

SUMMARY

Neurotransmission involves the exo-endocytic cycling of synaptic vesicles (SVs) within nerve terminals. Exocytosis is facilitated by a cytomatrix assembled at the active zone (AZ). The precise spatial and functional relationship between exocytic fusion of SVs at AZ membranes and endocytic SV retrieval is unknown. Here, we identify the scaffold G protein coupled receptor kinase 2 interacting (GIT) protein as a component of the AZ-associated cytomatrix and as a regulator of SV endocytosis. GIT1 and its *D. melanogaster* ortholog, dGIT, are shown to directly associate with the endocytic adaptor stonin 2/stoned B. In *Drosophila dgIt* mutants, stoned B and synaptotagmin levels are reduced and stoned B is partially mislocalized. Moreover, *dgIt* mutants show morphological and functional defects in SV recycling. These data establish a presynaptic role for GIT in SV recycling and suggest a connection between the AZ cytomatrix and the endocytic machinery.

INTRODUCTION

Synaptic transmission involves the rapid calcium-triggered exocytosis of synaptic vesicles (SVs) at presynaptic active zones (AZs) (Gundelfinger and Fejtova, 2012; Haucke et al., 2011) followed by SV protein endocytosis at the rim of the AZ (Dittman and Ryan, 2009; Haucke et al., 2011). The AZ membrane is associated with an electron-dense protein matrix, termed the cytomatrix of the active zone (CAZ), that is partially resistant to detergent extraction (Phillips et al., 2001). CAZ components (Gundelfinger and Fejtova, 2012) include giant multidomain proteins such as piccolo, bassoon, ELKS (also termed CAST), relatives of *Drosophila* bruchpilot (BRP) (Kittel et al., 2006) and Fife (Bruckner et al., 2012), Rab3 interacting molecules (RIMs) (Kaesler et al., 2011), RIM binding proteins (RBPs) (Liu et al., 2011), Munc13, liprins, and G protein coupled receptor kinase

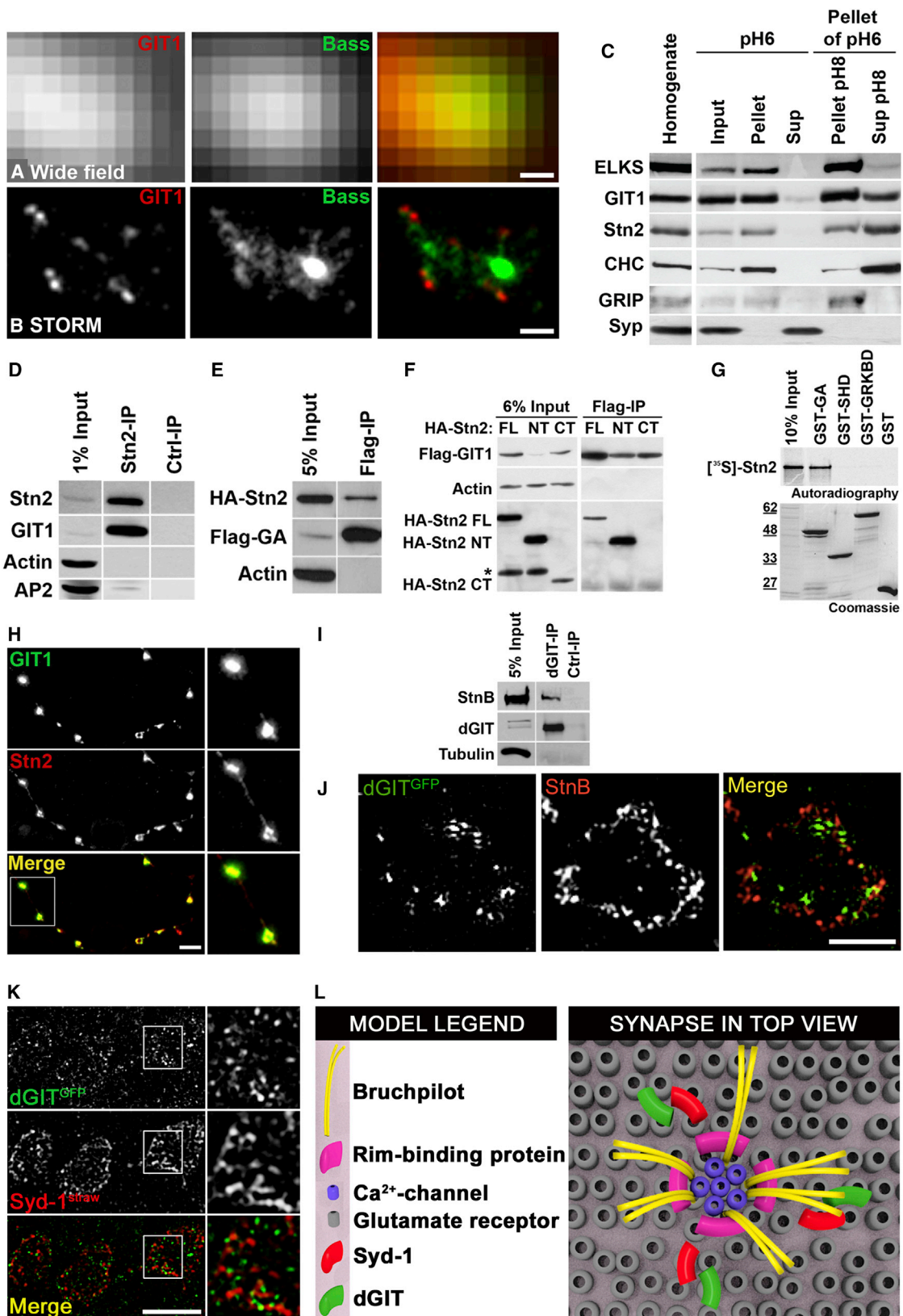
2 interacting protein (GIT) (Kim et al., 2003). Endocytic retrieval of exocytosed SV proteins involves adaptor proteins (Dittman and Ryan, 2009) such as AP-2, stonins (Fergestad and Broadie, 2001; Mullen et al., 2012), and AP180 (Koo et al., 2011). Stonin 2, the mammalian ortholog of *Drosophila* stoned B and of *C. elegans* unc-41 (Mullen et al., 2012), acts as a cargo-specific sorter for the SV calcium sensor synaptotagmin (Diril et al., 2006; Kononenko et al., 2013). The precise location and mechanisms of SV protein recapture and SV reformation remain enigmatic. Based on superresolution imaging, it was suggested that SV protein endocytosis may occur from the periaxial zone, a horse-shoe-shaped area surrounding the AZ center (Hua et al., 2011). Recent data indicate that SV exocytosis at AZs and SV endocytosis from the periaxial zone are functionally coupled (Haucke et al., 2011; Hosoi et al., 2009; Xu et al., 2013). The mechanism that underlies coupling, as well as the physical and functional relationship between the CAZ and the endocytic machinery, is poorly understood.

Here, we establish a presynaptic role for the AZ-associated scaffold protein GIT in SV endocytosis. Mammalian GIT1 harbors a GTPase activating domain for ADP ribosylation factor 6 (Arf6) and among other factors associates with CAZ components (Kim et al., 2003). We show that GIT plays a presynaptic role in stonin-mediated SV recycling, suggesting a physical and functional connection between the presynaptic AZ cytomatrix and the machinery for SV endocytosis. As GIT1 is genetically linked to attention-deficit hyperactivity disorder (ADHD) (Won et al., 2011), these findings are important for our understanding of neurological and neuropsychiatric diseases.

RESULTS

GIT Localizes to the Periphery of Presynaptic AZs and Binds to stonin 2/stoned B

GIT1 is involved in CAZ organization via its association with the AZ protein piccolo (Kim et al., 2003) and regulates endocytic membrane traffic (Claign et al., 2000), suggesting a potential presynaptic function in SV exo-endocytosis. Neither the localization nor the role of GIT1 in the presynapse has been studied so far. We therefore analyzed the localization of GIT1 and the AZ protein



(legend on next page)

bassoon at hippocampal synapses. Since the size of AZs is below the diffraction limit of resolution (Figure 1A), we employed multicolor spectral demixing direct stochastic optical reconstruction microscopy (SD-*d*STORM) with a lateral resolution of 25 nm (Lampe et al., 2012). GIT1 localized to distinctive puncta at the periphery of the AZ center defined by bassoon (Figure 1B), with a mean peak distance between individual bassoon spots and GIT1 of 76 ± 8 nm (SEM, $n = 30$ synapses), which is similar to that measured by STORM for bassoon and the AZ protein RIM1 (mean \pm SEM $\sim 40 \pm 5$ nm), but much smaller than the distance between bassoon and the postsynaptic protein Homer1 (mean \pm SEM $\sim 154 \pm 1.2$ nm) (Dani et al., 2010). To confirm the association of GIT1 with the CAZ, we used a biochemical approach for the enrichment of detergent-resistant proteins that may represent a biochemical correlate of the CAZ (Phillips et al., 2001). Detergent extraction of synaptosomes at pH 6 renders the majority of pre- and postsynaptic scaffolds, including CAZ components, insoluble. Re-extraction at elevated pH partially solubilizes proteins of the presynaptic CAZ. As expected for CAZ components, the majority of GIT1 and the BRP-related AZ protein ELKS remained detergent insoluble at pH 6, whereas the SV protein synaptophysin was solubilized completely (Figure 1C). Re-extraction of the insoluble pH 6 pellet at pH 8 solubilized a small fraction of GIT1 and ELKS, whereas postsynaptic GRIP remained insoluble (Figure 1C). Thus, GIT1 exhibits a partitioning behavior similar to that of the known AZ protein ELKS, confirming its association with the CAZ at mammalian synapses.

To further dissect a presynaptic role for GIT1 in SV exo-endocytosis, we aimed to identify presynaptic binding partners. Because reliable anti-GIT1 suitable for immunoprecipitation were unavailable, we screened a variety of well-characterized antibodies against known presynaptic proteins for their ability to coimmunoprecipitate GIT1 using tandem mass spectrometry (MS/MS)-based proteomics as a readout. These experiments identified GIT1 as a possible binding partner of the endocytic adaptor stonin 2 (Figure 1D). Further biochemical analysis using different truncation mutants (Figure S1G) revealed that the inter-

action between stonin 2 and GIT1 is direct (Figure 1G) and mediated by the ArfGAP-ankyrin repeat domain of GIT1 (Figures 1E and S1A) and the N-terminal domain (NT, aa 1–555) of stonin 2 (Figure 1F). Further, the conserved stonin-homology domain (StHD, aa 411–553) of stonin 2 on its own was unable to bind to GIT1, as was the related nonneuronal protein stonin 1 (Figures S1A and S1B). When expressed in mammalian cells, stonin 2-NT also bound to GIT2, but was unable to associate with non-GIT family ArfGAPs such as ACAP1 (Figure S1C). We observed no significant effects of stonin 2 on the ArfGAP activity of GIT1 (Figure S1H), suggesting that the GIT-stonin complex may serve a structural rather than an enzymatic role. We also probed whether complex formation between GIT and stonin family members is evolutionarily conserved. dGIT coimmunoprecipitated with the sole stonin family protein, stoned B, from *Drosophila* head extracts (Figure 1I), and this association was mediated by the ArfGAP-ankyrin repeat domain of dGIT (Figure S1D), similar to what was observed for mammalian GIT1. The evolutionary conservation of complex formation between GIT and stonin is underscored by the ability of *Drosophila* stoned B to bind to human GIT1 (Figure S1E) and of dGIT to associate with human stonin 2-NT (Figure S1F).

To corroborate these biochemical data, we studied the localization of GIT and stonin 2/stoned B in primary hippocampal neurons and at *Drosophila* larval neuromuscular junctions (NMJs). In hippocampal neurons in culture, GIT1 was concentrated at and around bassoon-containing presynaptic sites (Figure S1I), where it colocalized with stonin 2 (Figure 1H). Moreover, stonin 2 together with GIT1 and the endocytic protein clathrin (Phillips et al., 2001) partitioned to the detergent-insoluble CAZ in biochemical fractionation experiments (Figure 1C). Superresolution, dual-color, structured illumination microscopy imaging of *Drosophila* larval NMJs showed endogenous stoned B to be closely apposed to transgenically expressed dGIT-GFP (a construct that rescues dGIT loss of function [see below]; Figure 1J). To precisely define the localization of dGIT with respect to the AZ, we used dual-color stimulated emission depletion (STED) nanoscopy with a lateral resolution of 20 nm (Göttfert

Figure 1. GIT Localizes to the Edge of AZs and Directly Binds to stonin 2/stoned B

(A and B) GIT1 localizes to distinctive puncta at the periphery of the AZ center. Cultured hippocampal neurons (DIV14) costained for GIT1 (red) and bassoon (Bass, green) shown in wide field (A) or SD-*d*STORM (B). Scale bars, 200 nm.

(C) GIT1 is part of a detergent-resistant presynaptic matrix. Synaptosomes were extracted with 1% Triton X-100 at pH 6. The insoluble pellet was re-extracted with 1% Triton X-100 at pH 8. Equal amounts of soluble material (sup) and insoluble material (pellet) were analyzed by immunoblotting against the AZ protein ELKS, GIT1, stonin 2 (Stn2), clathrin heavy chain (CHC), synaptophysin (Syn), or the postsynaptic scaffold GRIP.

(D) Analysis of immunoprecipitates with antibodies against stonin 2 (Stn2), GIT1, actin, or AP2 (negative controls). GIT1 was coimmunoprecipitated with anti-Stn2 antibodies (Stn2-IP), but not control immunoglobulin G (IgG; Ctrl-IP).

(E) The FLAG-tagged ArfGAP-ankyrin repeat domain (GA) of GIT1 coimmunoprecipitates hemagglutinin-Stn2 (HA-Stn2) from transfected Cos7 cells.

(F) GIT1 associates with the NT domain of Stn2 in immunoprecipitates. FL, Stn2-full length; CT, Stn2 C-terminal domain.

(G) In vitro-translated Stn2 directly binds to the GA domain of GIT1. GST-GIT1 truncation mutants (GA, Spa2 homology domain [SHD]), and G protein receptor kinase binding domain [GRKBD]) were used to pull down in vitro-translated [35 S]-Stn2.

(H) Colocalization of endogenous GIT1 (green) with HA-tagged stonin 2 (Stn2, red) at synapses of primary hippocampal neurons in culture (DIV14). Scale bar, 5 μ m.

(I) Coimmunoprecipitation of dGIT with stoned B (StnB) from *D. melanogaster* head extracts using dGIT antibodies (dGIT-IP). Ctrl-IP, preimmune IgG.

(J) StnB is closely apposed to transgenically expressed dGIT-GFP at *Drosophila* larval NMJs. dGIT-GFP-expressing NMJs were immunostained with antibodies against StnB and GFP and imaged by structured illumination microscopy. Scale bar, 2 μ m.

(K) Single-layer STED images showing the localization of dGit^{GFP} in relation to Syd-1^{straw} at the *Drosophila* larval NMJ. Anti-GFP and anti-DsRed immunoreactivity was observed in close proximity to each other, indicating that dGIT is positioned in the periphery of the AZ. Scale bar, 2 μ m.

(L) Model of an AZ in top view, showing the position of the indicated proteins in relationship to each other.

See also Figure S1.

et al., 2013). STED-based nanoscopy revealed dGIT to be localized to the rim of presynaptic AZs closely interspaced with Syd-1, a scaffold of the AZ periphery surrounding BRP at the AZ center (Owald et al., 2010; Figures 1K and 1L). Thus, the precise localization of GIT at both glutamatergic hippocampal synapses and glutamatergic *Drosophila* NMJs appears very similar. These results show that GIT and stonin 2/stoned B associate with the CAZ, directly bind to each other, and localize to the periphery of AZs at presynaptic sites.

GIT Regulates the Localization and Function of stonin 2/stoned B at Synapses

Mammalian genomes contain two similar GIT genes (encoding GIT1 and GIT2) that likely overlap functionally. Moreover, mammalian GIT1 regulates synapse formation and postsynaptic spine morphogenesis (Menon et al., 2010; Segura et al., 2007), compromising analysis of a possible presynaptic function of GIT1/2 in vivo. To circumvent these problems when analyzing the role of GIT at the presynapse in vivo, we decided to subject the single *Drosophila digit* locus to genetic manipulation (Figure S2A). Using transposon-mediated excision, we deleted major parts of dGIT (eliminating expression of the Spa2 homology domain [SHD] and paxillin-binding site [PBS] domain) together with the neighboring gene (CG11833; Figure S2A). To remove dGIT function from flies, we placed the resulting chromosome (*digitex10*) over a piggy Bac transposon insertion located within the *digit* locus (*digitf03586*). In the resulting transheterozygous mutants (*digitex10/digitf03586*; hereafter referred to as *digit f03*), dGIT function was specifically eliminated. A second dGIT loss-of-function mutant was generated by placing *digitex10* over a large deficiency *Df(2R)Df596* (*digitex10/Df(2R)Df596*; referred to as *digit Df*). Both mutants displayed undetectable dGIT protein expression in fly head extracts (Figure 2A) and reduced adult viability (not shown). Moreover, locomotion assessed by negative geotaxis was similarly affected in both alleles (*digit Df* and *digit f03*; Figure 2B). Importantly, these phenotypes were rescued by transgenic neuronal (e.g., presynaptic) re-expression of dGIT or GFP-dGIT under the panneuronal *elav-Gal4* driver (see Figure 2B and below). Thus, defects in locomotion can be assigned to a loss of dGIT function in the nervous system and specifically within the presynaptic compartment.

The physical association of dGIT with stoned B suggests a possible functional relationship between the two proteins. Quantitative immunoblotting revealed that stoned B levels were significantly reduced in head extracts from *digit f03* mutant animals, whereas expression of other endocytic proteins, such as Dap160/intersectin and dynamin, were unaltered (Figures 2C–2F). To probe whether similar alterations may occur at the level of presynaptic boutons, we analyzed the expression or localization of synaptic proteins at *Drosophila* larval NMJs. Quantification of the levels of various pre- and postsynaptic proteins in *digit* mutant NMJs revealed a significant and specific decrease in the amount of stoned B, a phenotype that was fully rescued by presynaptic re-expression of dGIT. In contrast, no change in the amount of the endocytic protein Dap160/intersectin was found in either genotype (Figures 2G–2I). We then analyzed the localization and expression of the SV proteins CSP and synaptotagmin 1, the AZ protein BRP, and postsynaptic glutamate re-

ceptors (Figure S2B). Stoned B has previously been shown to be required for proper expression and endocytic sorting of synaptotagmin in flies and mammals (Diril et al., 2006; Fergestad and Broadie, 2001; Stimson et al., 2001). Presynaptic expression of synaptotagmin 1 was indeed reduced in *digit* mutants compared with controls, akin to what was observed for stoned B mutants (Fergestad and Broadie, 2001; Stimson et al., 2001), and this was rescued by re-expression of dGIT (Figures 2J and S2B). By contrast, the levels of CSP or BRP were unaltered in *digit* mutant animals (Figures 2K, 2M, and S2B). Endocytic mis-sorting of synaptotagmin, similar to loss of function of stoned B in *Drosophila* or of stonin 2 in mice (Kononenko et al., 2013), was also observed in hippocampal neurons expressing synaptotagmin 1-pHluorin depleted of endogenous GIT1 by small interfering RNA (siRNA; Figures S4D and S4E). Thus, the function of the dGIT/GIT1-stoned B/stonin 2 complex seems to be evolutionarily conserved. Postsynaptic glutamate receptor fields were enlarged in *digit* mutant NMJs, a phenotype rescued by motoneuron-specific re-expression of dGIT (Figures 2L and S2B). A similar enlargement of glutamate receptor fields (juxtaposed with presynaptic AZs) was observed previously in other mutants that affect CAZ integrity (e.g., *syd-1* and *brp*) (Kittel et al., 2006; Oswald et al., 2010).

Loss of *digit* not only resulted in reduced presynaptic expression of stoned B but also caused a partial, yet significant redistribution of stoned B from cortical areas of presynaptic boutons toward the lumen, indicating that dGIT regulates proper subsynaptic targeting of stoned B (Figures S2C and S2D), whereas Dap160/intersectin distribution appeared unaffected. These results show that GIT regulates the localization and function of stonin 2/stoned B at synapses.

Accumulation of Enlarged Vesicles at *digit* Mutant Synapses

Drosophila stoned mutants not only display defects with respect to synaptotagmin expression but also show morphological abnormalities within their NMJs, most notably an accumulation of enlarged (>100 nm) endocytic vesicles (Fergestad and Broadie, 2001; Stimson et al., 2001). To probe for possible ultrastructural alterations during SV cycling, we stimulated wild-type (WT) or *digit f03* mutant larvae and, following a brief period of recovery, analyzed their presynaptic ultrastructure by electron microscopy (EM)-based morphometry. Synapses from *digit* mutants appeared largely unaltered (Figures 3A–3D), with no change in the numbers of SVs (Figure 3E) or SVs docked to the presynaptic membrane (Figure 3F). Moreover, *digit* mutants displayed a normal size (Figure 3G) and structure of the CAZ, as well as a normal organization of T-bars (Figures 3C and 3D) and the SVs tethered to them (Figures 3C–3F). However, *digit* mutant terminals showed an accumulation of endosomal structures and vacuoles (i.e., >80 nm vesicles or cisternae; Figures 3A–3D and 3H; Table S1) similar to the cisternae observed in *stoned* and in *shibire^{ts}* mutants following release from temperature block. The increased endosome area per bouton was rescued completely by neuron-specific re-expression of dGIT ([$\mu\text{m}^2/\mu\text{m}^2$]: control: 0.020 ± 0.004 ; *digit f03*: $0.039 \pm 0.008^*$, $p \leq 0.04$; *digit f03*-rescue: 0.023 ± 0.005 , insignificantly different from control), indicating that the defect originates from presynaptic loss of dGIT (Figure 3H).

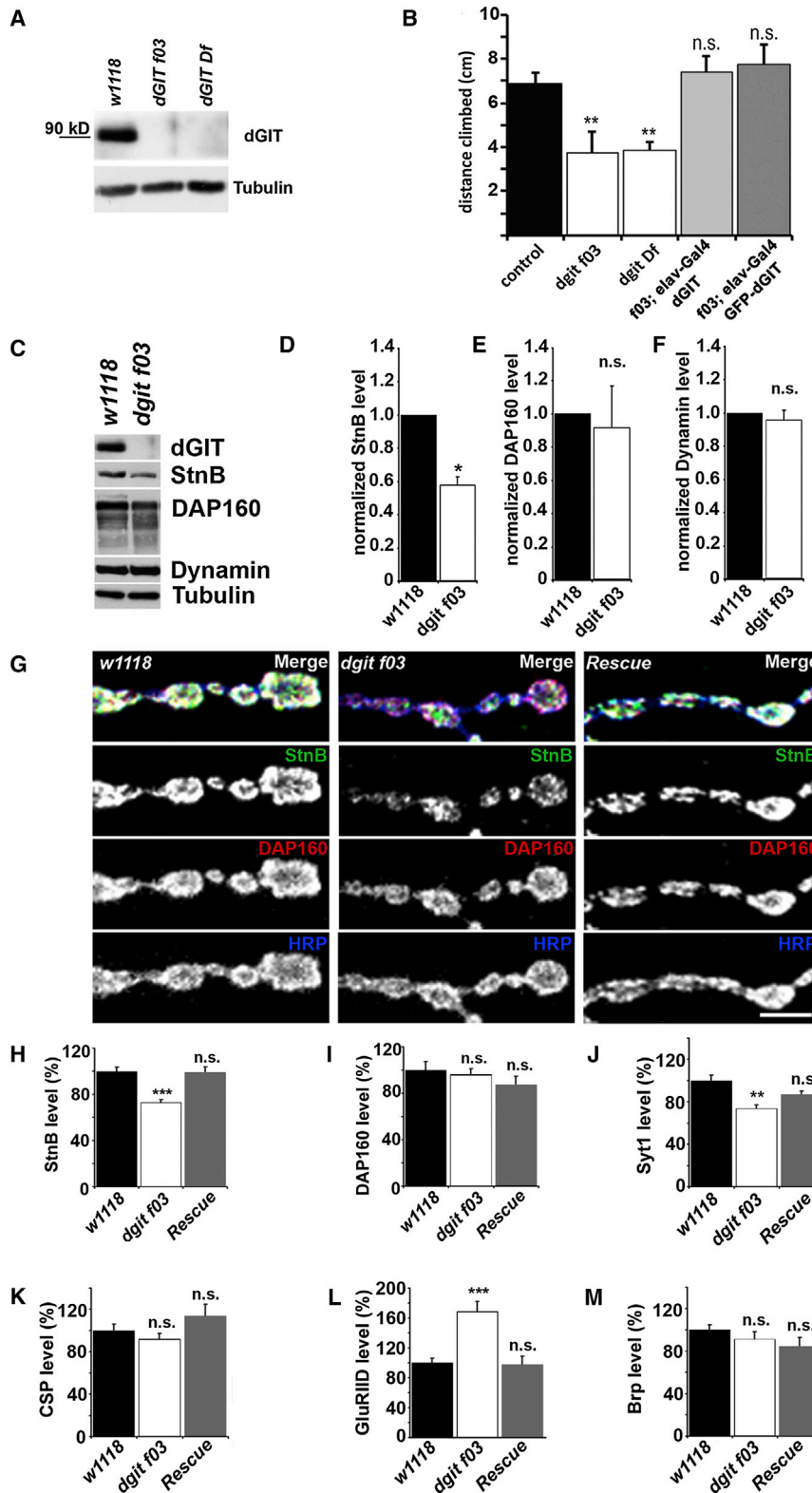


Figure 2. dGIT Regulates Presynaptic Levels and Localization of StnB and Synaptotagmin 1 at *Drosophila* NMJ Synapses

(A) Immunoblot analysis of fly head lysates. dGIT is present in WT (*w¹¹¹⁸/elav-Gal4*) but undetectable in *dgIt* mutants (*DgIt Df: elav-Gal4/+; dgItDf596/10* and *DgIt f03: elav-Gal4/+; f03568/10*). Tubulin, control.

(B) Locomotion was analyzed in control *w¹¹¹⁸/elav-Gal4*, *dgIt* mutants, and *rescue* adult flies after the flies' wings were clipped. *dgIt f03* and *Df* mutants showed decreased negative geotaxis as quantified by the mean distance climbed vertically within 30 s. Control: *w¹¹¹⁸/elav-Gal4* (*n* = 24). *DgIt Df: elav-Gal4/Y; dgItDf596/10* (*n* = 15). *DgIt f03: elav-Gal4/Y; dgItf03586/10* (*n* = 14). *f03; UAS dgIt: elav-Gal4/Y; dgIt10/f03586; UAS-dGIT/+* (*n* = 10). *f03; UAS GFP-dgIt: elav-Gal4/Y; dgIt10/f03586; UAS-GFP::dGIT/+* (*n* = 9; mean \pm SEM).

(C–F) Reduced levels of stoned B (StnB) in head extracts from *dgIt f03* mutant flies.

(C) Fly head extracts (five heads per lane) from adult *w¹¹¹⁸/elav-Gal4* or *dgIt* mutants flies (*dgIt f03/elav-Gal4/+; f03568/10*) were analyzed by quantitative immunoblotting against the indicated proteins.

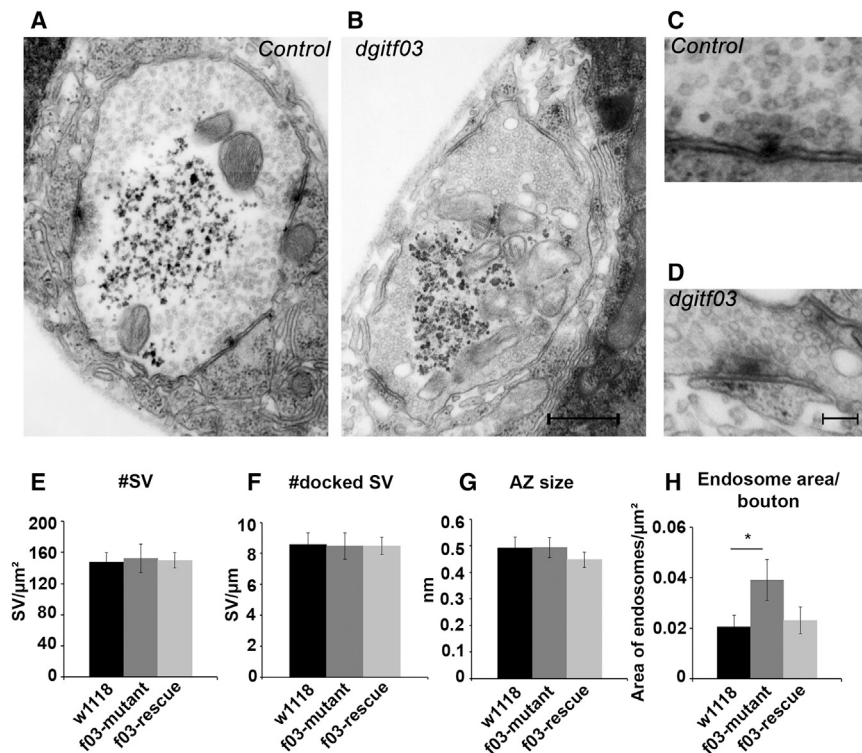
(D–F) StnB is reduced (D; *dgIt f03*: 0.58 ± 0.05 , *p* = 0.0132), whereas Dap160/intersectin (E; *dgIt f03*: 0.91 ± 0.25 , *p* = 0.7691, n.s.) and dynamin (F; *dgIt f03*: 0.96 ± 0.06 , *p* = 0.5528, n.s.) are unchanged (mean \pm SEM, *n* \geq 2 experiments).

(G) StnB levels are reduced at dGIT mutant NMJs, a phenotype rescued by presynaptic reexpression of dGIT. Muscle 4 NMJ from WT (*w¹¹¹⁸*), dGIT mutant (*dgIt f03*), and *dgIt rescue* larvae immunostained for StnB (green), Dap160/intersectin (red), and horseradish peroxidase (blue) are shown. Scale bar, 4 μ m.

(H and I) Quantification of data in (G). The levels of StnB are significantly decreased in *dgIt* mutants (H; *w¹¹¹⁸*: 100 ± 3.7 , *n* = 28; *dgIt f03*: 73.1 ± 2.5 , *n* = 31, *p* < 0.0001; *rescue*: 98.8 ± 5.1 , *n* = 19, *p* = 0.847), whereas Dap160/intersectin remains unchanged (I; *w¹¹¹⁸*: 100 ± 7.4 , *n* = 17; *dgIt f03*: 96.3 ± 4.9 , *n* = 22, *p* = 0.671; *rescue*: 87.4 ± 7.3 , *n* = 14, *p* = 0.242). Mean \pm SEM.

(J–M) Quantification of pre- and postsynaptic protein levels at NMJs from WT (*w¹¹¹⁸*), dGIT mutant (*dgIt f03*), and *dgIt rescue* larvae. Levels of synaptotagmin 1 (Syt1) are reduced in *dgIt* mutants (J; *w¹¹¹⁸*: 100 ± 4.9 , *n* = 18; *dgIt f03*: 73.7 ± 3.6 , *n* = 17, *p* = 0.0002; *rescue*: 86.5 ± 3.7 , *n* = 12, *p* = 0.056). Levels of CSP (K; *w¹¹¹⁸*: 100 ± 6.1 , *n* = 30; *dgIt f03*: 92.2 ± 5.2 , *n* = 27, *p* = 0.340; *rescue*: 113.8 ± 11.2 , *n* = 28, *p* = 0.276) or Brp (M; *w¹¹¹⁸*: 100 ± 4.6 , *n* = 19; *dgIt f03*: 91.0 ± 7.2 , *n* = 20, *p* = 0.306; *rescue*: 84.1 ± 8.7 , *n* = 18, *p* = 0.108) are unchanged, whereas glutamate receptor (GluRIID) levels are increased (L; *w¹¹¹⁸*: 100 ± 5.9 , *n* = 15; *dgIt f03*: 168.6 ± 13.6 , *n* = 17, *p* = 0.0001; *rescue*: 97.4 ± 11.2 , *n* = 15, *p* = 0.843). Mean \pm SEM. Scale bar, 4 μ m.

See also Figure S2.



To explore whether these ultrastructural alterations in *digit* mutants are linked to functional deficits in neurotransmission, we performed two electrode voltage-clamp recordings of late third-instar larval NMJs. Evoked excitatory junctional currents (eEJCs) were significantly reduced in *digit f03* mutant larvae compared with controls, a defect that was rescued by presynaptic re-expression of UAS-*digit* using the motoneuronal driver *ok6-GAL4* (Figure S3A). No significant changes in the rise times and decay constants τ of evoked responses or in the amplitude of spontaneous miniature currents were observed (Figures S3B and S3C), whereas mEJC frequency was slightly but insignificantly increased (Figure S3D). The mEJC rise time and decay constant τ were also unaltered in *git f03* mutants (mEJC rise time, control: 0.85 ± 0.05 , $n = 13$; *digit f03*: 0.78 ± 0.05 , $n = 11$; $p = 0.31$; Student's *t* test; mEJC τ , control: 7.6 ± 0.5 , $n = 13$; *digit f03*: 7.3 ± 0.5 , $n = 11$; $p = 0.77$; Student's *t* test). Overall, these data show that loss of *digit* phenocopies the ultrastructural and functional defects observed in *stoned* mutants, further supporting the close physical and functional association of both proteins within the SV cycle.

dGIT Regulates SV Recycling

To probe the putative function of dGIT in SV cycling more directly, we stimulated larval NMJs under depolarizing conditions and monitored SV endocytosis using the styryl dye FM1-43. The amount of FM1-43 that is incorporated serves as a measure for the efficacy of membrane retrieval and thus SV recycling (Verstreken et al., 2008). Control boutons revealed strongly incorporated FM dye, whereas *digit f03* or *digit Df* mutant boutons loaded FM1-43 with a significantly reduced efficiency.

This apparent defect in SV recycling was rescued by presynaptic re-expression of dGIT (Figures 4A–4G). To dissect a primary role of dGIT in exocytosis from a function in endocytic membrane retrieval, we measured evoked neurotransmission and FM1-43 uptake under conditions of elevated extracellular calcium, which invariably results in a high release probability (Miśkiewicz et al., 2011). Under these conditions, evoked neurotransmission of *digit f03* mutants did not differ significantly from that of WT controls, whereas FM1-43 uptake was significantly reduced (Figures S4A and S4B), suggesting that defective FM1-43 uptake primarily results from impaired endocytosis or SV recycling.

To further characterize the role of dGIT in SV endocytosis, we transgenically expressed synapto-pHluorin, a chimeric SV protein whose fluorescence is low in the acidic environment of the SV lumen and high when it is exocytosed to the cell surface (Miesenböck et al., 1998). The WT controls and *digit f03* mutant animals showed identical synapto-pHluorin expression, as revealed by quantification of synaptic fluorescence levels following application of ammonium chloride to alkalize the lumen of SVs (Figure S4C). To systematically investigate possible endocytosis defects, we stimulated exo-endocytosis with action potential (AP) trains at different frequencies (10 Hz and 50 Hz), which invariably resulted in a transient rise and subsequent decay of synapto-pHluorin fluorescence in synaptic boutons. Experiments were performed in 5 mM extracellular CaCl₂, which ensured a similar extent of stimulus-induced exocytosis (normalized maximal fluorescence following blockage of SV reacidification with folimycin: 100 APs at 10 Hz: control = (100 ± 10)%, *digitf03* = (101 ± 6)%; 100 APs at 50 Hz: control = (100 ± 20)%, *digitf03* = (105 ± 25)%, $n = 3$ animals and $n = 15$ boutons), allowing us to study a possible involvement of dGIT in SV endocytosis and postendocytosis processing of internalized membranes independent of its function in exocytosis (see above). Strikingly,

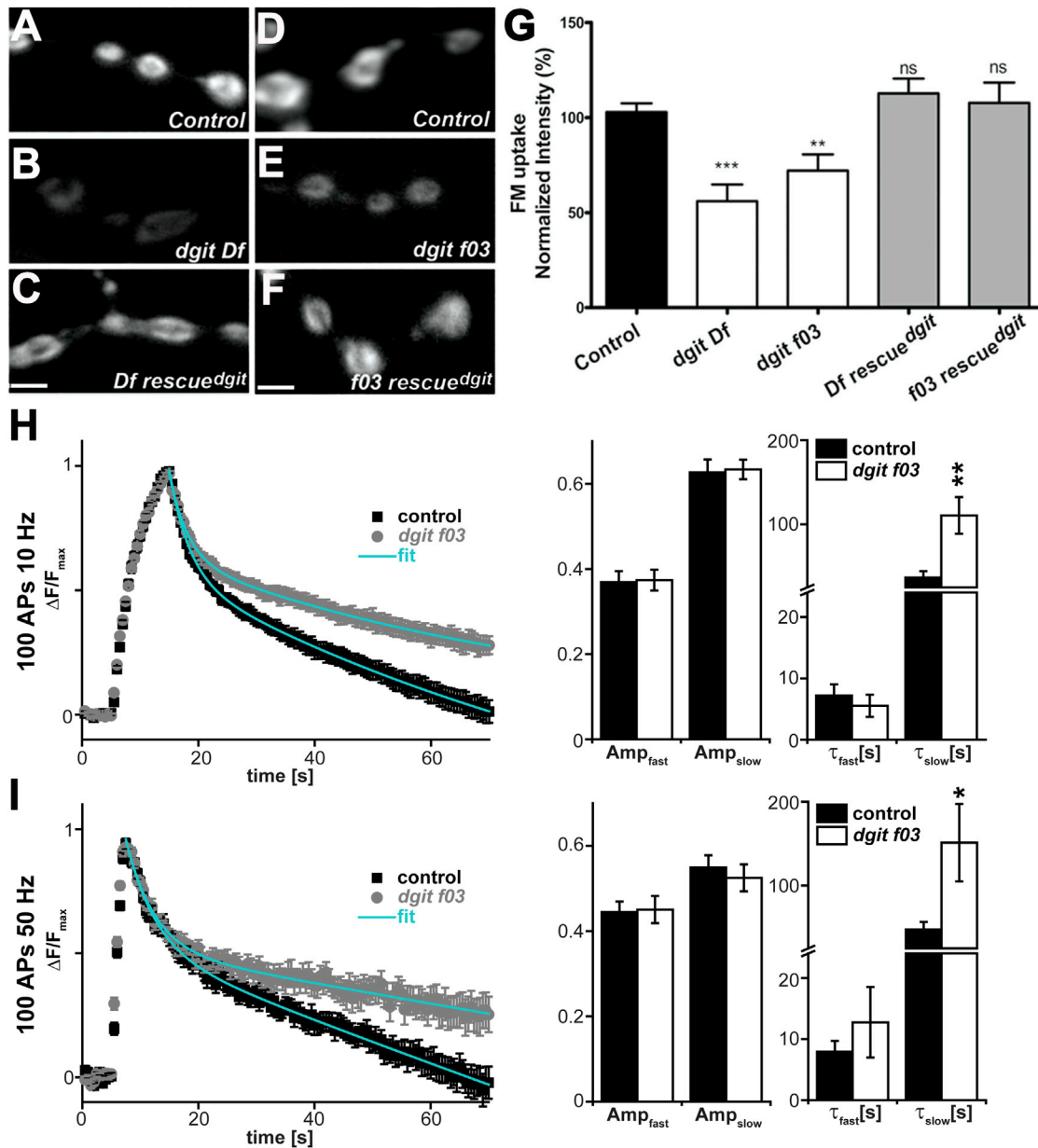


Figure 4. dGIT Regulates SV Recycling

(A–F) FM dye uptake is reduced in *dgitt* mutants. FM1–43 dye uptake in control (*w1118/OK6-Gal4*; A and D), *dgitt* mutants (*dgitt f03* and *dgitt Df*; B and E), and the corresponding rescued larvae (*f03 rescue^{dgitt}* or *Df rescue^{dgitt}*; C and F). Third instar larval NMJs were incubated in 4 μ M FM1–43 and stimulated for 5 min with 90 mM KCl, 1.5 mM CaCl₂. Scale bar, 2 μ m.

(G) Quantification of FM1–43 dye uptake (mean \pm SEM, $n \geq 12$ NMJs). Student's *t* test, ***p* < 0.01, ****p* < 0.001; ns, not significant.

(H) Left: exo-endocytosis and vesicle reacidification assayed by synaptopHluorin (SpH). Time-dependent fluorescence changes in response to stimulation with 100 APs at 10 Hz (starting at *t* = 5 s) in control (black, *OK6/+*; *UAS-SpH/+*) and *dgitt f03* (gray, *fo3/ex10,OK6*; *UAS-SpH/+*) boutons. The cyan trace is a fit with a double exponential function. Right: kinetic analysis of the bimodal endocytosis/reacidification assayed by SpH. The relative contributions of the fast (Amp_{fast}) and slow (Amp_{slow}) components, as well as the respective time constants (τ_{fast} and τ_{slow}), are shown.

(I) Same as (H), but for a stimulation of 100 APs at 50 Hz. Data in (H) and (I) are mean \pm SEM from $n \geq 4$ animals with 5 boutons per animal; **p* < 0.05, ***p* < 0.01, two-tailed *t* test.

See also Figure S4.

normalized fluorescence traces revealed a slowing of the average synapto-pHluorin fluorescence decay in *dgitt* mutants (Figures 4H and 4I). To scrutinize this effect further, we investi-

gated the temporal properties of the postexocytosis synapto-pHluorin signals. Fitting of exponentials revealed that the fluorescence decay in both genotypes was well described by a

double exponential function (cyan lines in Figures 4H and 4I), indicative of bimodal kinetics with a fast and a slow component. Quantification of parameters obtained by kinetic analysis of traces from individual boutons revealed that the relative amplitudes of the fast and slow components (Amp_{fast} and Amp_{slow} , respectively, in Figures 4H and 4I) were indistinguishable between control and mutant synapses. Moreover, no significant difference between the fast time constants (τ_{fast} in Figures 4H and 4I) was found, suggesting that this component functions independently of dGIT. In contrast, the time constant of the slow component (τ_{slow} in Figures 4H and 4I) was specifically and significantly increased in *dgIt* mutants. These data indicate that dGIT is essential to ensure the efficacy of the slow phase of endocytosis and SV reacidification, which in our hands predominates postexocytosis processing ($Amp_{slow} > Amp_{fast}$). This provides a mechanistic explanation for the endocytic defects observed by EM and FM1-43 dye uptake experiments in the absence of dGIT.

Collectively, our results unravel a presynaptic role of GIT in SV recycling that is linked at least in part to its ability to regulate the expression level and localization of the synaptotagmin-specific endocytic sorting adaptor stonin 2/stoned B.

DISCUSSION

We have shown here that the CAZ-associated protein GIT physically and functionally associates with the endocytic adaptor stonin2/stoned B (Figure 1). Loss of function of dGIT in *Drosophila* leads to reduced levels of stoned B and its endocytic cargo synaptotagmin (Figure 2) and to endocytic defects (Figures 3 and 4), a phenotype that resembles that of *stoned* mutants. Presynaptic rescue experiments further demonstrate that the presynaptic role of GIT is independent of its established postsynaptic functions (Bahri et al., 2009; Zhang et al., 2005). These data, together with the localization of stonin at the periphery of AZs (Figure 1) and with the partitioning of stonin and several other endocytic proteins into detergent-resistant fractions containing CAZ proteins such as ELKS and GIT1 (Figure 1; Phillips et al., 2001), favor a hypothetical model in which GIT acts as a molecular bridge for the recruitment of stonin 2/stoned B to the periphery of the AZ. Physical connections between the AZ-based exocytic apparatus and the endocytic machinery may regulate vesicle reformation and thus availability, thereby contributing to efficient SV exo-endocytic cycling (Haucke et al., 2011; Hosoi et al., 2009; Sakaba et al., 2013; Xu et al., 2013). Our finding that *dgIt* mutants show a selective defect in the slow component of SV recycling and reacidification (Figure 4) is explained best by a speculative model according to which exocytosed SV membranes are internalized via clathrin-dependent (Granseth et al., 2006) and clathrin-independent (Watanabe et al., 2013) pathways, the latter of which results in the formation of endosomal vacuoles from which SVs are regenerated. Loss of *dgIt* in this model does not affect membrane retrieval per se, but selectively impairs slow, presumably clathrin- (Heerssen et al., 2008) and stoned B-mediated reformation of acidified SVs. We thus favor a hypothetical scenario in which the dGIT-stoned B complex in conjunction with other factors regulates SV reformation from internalized endosomal structures in order to replenish SVs close to the AZ (as recently

observed at mammalian synapses; Schikorski, 2014). Further studies are required to put this model to the test. As GIT1 has been implicated in neuropsychiatric diseases such as ADHD (Won et al., 2011), the results reported here raise the possibility that GIT-dependent changes in presynaptic function may underlie ADHD-like disease in mice and men.

EXPERIMENTAL PROCEDURES

Confocal Microscopy of NMJs

Dissection, immunostaining, and confocal imaging of larval NMJs were done as described previously (Fouquet et al., 2009). Stacks from third instar larval muscle 4 (step size 0.5 μ m) were acquired with a Leica TCS-SP5 microscope and a 63 \times 1.4 NA oil objective (Leica) under the control of Application Suite Advanced Fluorescence (LAS-AF; Leica) software. ImageJ was used for maximum projections of stacks, quantification of areas, and fluorescence intensity profiles. To assess the distribution of endocytic proteins within boutons in Figures S2C and S2D, line scans were used to define the cortex of the bouton. Fluorescence intensities/area were measured for the bouton cortex versus the bouton lumen and set to one for WT larval NMJs.

Statistics

Data were analyzed by unpaired Student's *t* test or a one-way ANOVA using GraphPad. Data represent mean \pm SEM, and *n* indicates the number of samples examined. Asterisks denote significance (n.s., *p* > 0.05; **p* < 0.05; ***p* < 0.001; ****p* < 0.0001).

For further information regarding the materials and methods used in this work, see Supplemental Experimental Procedures.

SUPPLEMENTAL INFORMATION

Supplemental Information includes Supplemental Experimental Procedures, four figures, and one table and can be found with this article online at <http://dx.doi.org/10.1016/j.celrep.2014.04.051>.

ACKNOWLEDGMENTS

We thank Drs. P.A. Randazzo (NIH), V. Hsu (Harvard Medical School), O. Shupliakov (Karolinska Institute), and N.E. Reist (Colorado State University) for reagents and Prof. S.W. Hell and F. Göttfert for help with STED microscopy. This work was supported by grants from the DFG (SFB958/A01 and HA2686/4-1 to V.H., SFB958/Z02 to J.S., and SFB958/A03 and SFB958/A06 to S.J.S.) and the Chinese funding agency NSFC (30930033 and 31110103907 to Y.Q.Z.).

Received: October 1, 2013

Revised: April 9, 2014

Accepted: April 23, 2014

Published: May 29, 2014

REFERENCES

- Bahri, S.M., Choy, J.M., Manser, E., Lim, L., and Yang, X. (2009). The *Drosophila* homologue of Arf-GAP GIT1, dGIT, is required for proper muscle morphogenesis and guidance during embryogenesis. *Dev. Biol.* 325, 15–23.
- Bruckner, J.J., Gratz, S.J., Slind, J.K., Geske, R.R., Cummings, A.M., Galindo, S.E., Donohue, L.K., and O'Connor-Giles, K.M. (2012). Fife, a *Drosophila* Piccolo-RIM homolog, promotes active zone organization and neurotransmitter release. *J. Neurosci.* 32, 17048–17058.
- Claing, A., Perry, S.J., Achiriloaie, M., Walker, J.K., Albanesi, J.P., Lefkowitz, R.J., and Premont, R.T. (2000). Multiple endocytic pathways of G protein-coupled receptors delineated by GIT1 sensitivity. *Proc. Natl. Acad. Sci. USA* 97, 1119–1124.
- Dani, A., Huang, B., Bergan, J., Dulac, C., and Zhuang, X. (2010). Superresolution imaging of chemical synapses in the brain. *Neuron* 68, 843–856.

- Diril, M.K., Wienisch, M., Jung, N., Klingauf, J., and Haucke, V. (2006). Stonin 2 is an AP-2-dependent endocytic sorting adaptor for synaptotagmin internalization and recycling. *Dev. Cell* 10, 233–244.
- Dittman, J., and Ryan, T.A. (2009). Molecular circuitry of endocytosis at nerve terminals. *Annu. Rev. Cell Dev. Biol.* 25, 133–160.
- Fergestad, T., and Broadie, K. (2001). Interaction of stoned and synaptotagmin in synaptic vesicle endocytosis. *J. Neurosci.* 21, 1218–1227.
- Fouquet, W., Oswald, D., Wichmann, C., Mertel, S., Depner, H., Dyba, M., Haltermann, S., Kittel, R.J., Eimer, S., and Sigrist, S.J. (2009). Maturation of active zone assembly by *Drosophila* Bruchpilot. *J. Cell Biol.* 186, 129–145.
- Göttfert, F., Wurm, C.A., Mueller, V., Berning, S., Cordes, V.C., Honigmann, A., and Hell, S.W. (2013). Coaligned dual-channel STED nanoscopy and molecular diffusion analysis at 20 nm resolution. *Biophys. J.* 105, L01–L03.
- Granseth, B., Odermatt, B., Royle, S.J., and Lagnado, L. (2006). Clathrin-mediated endocytosis is the dominant mechanism of vesicle retrieval at hippocampal synapses. *Neuron* 51, 773–786.
- Gundelfinger, E.D., and Fejtova, A. (2012). Molecular organization and plasticity of the cytomatrix at the active zone. *Curr. Opin. Neurobiol.* 22, 423–430.
- Haucke, V., Neher, E., and Sigrist, S.J. (2011). Protein scaffolds in the coupling of synaptic exocytosis and endocytosis. *Nat. Rev. Neurosci.* 12, 127–138.
- Heerssen, H., Fetter, R.D., and Davis, G.W. (2008). Clathrin dependence of synaptic-vesicle formation at the *Drosophila* neuromuscular junction. *Curr. Biol.* 18, 401–409.
- Hosoi, N., Holt, M., and Sakaba, T. (2009). Calcium dependence of exo- and endocytotic coupling at a glutamatergic synapse. *Neuron* 63, 216–229.
- Hua, Y., Sinha, R., Thiel, C.S., Schmidt, R., Hüve, J., Martens, H., Hell, S.W., Egner, A., and Klingauf, J. (2011). A readily retrievable pool of synaptic vesicles. *Nat. Neurosci.* 14, 833–839.
- Kaesler, P.S., Deng, L., Wang, Y., Dulubova, I., Liu, X., Rizo, J., and Südhof, T.C. (2011). RIM proteins tether Ca²⁺ channels to presynaptic active zones via a direct PDZ-domain interaction. *Cell* 144, 282–295.
- Kim, S., Ko, J., Shin, H., Lee, J.R., Lim, C., Han, J.H., Altmann, W.D., Garner, C.C., Gundelfinger, E.D., Premont, R.T., et al. (2003). The GIT family of proteins forms multimers and associates with the presynaptic cytomatrix protein Piccolo. *J. Biol. Chem.* 278, 6291–6300.
- Kittel, R.J., Wichmann, C., Rasse, T.M., Fouquet, W., Schmidt, M., Schmid, A., Wagh, D.A., Pawlu, C., Kellner, R.R., Willig, K.I., et al. (2006). Bruchpilot promotes active zone assembly, Ca²⁺ channel clustering, and vesicle release. *Science* 312, 1051–1054.
- Kononenko, N.L., Diril, M.K., Puchkov, D., Kintscher, M., Koo, S.J., Pfuhl, G., Winter, Y., Wienisch, M., Klingauf, J., Breustedt, J., et al. (2013). Compromised fidelity of endocytic synaptic vesicle protein sorting in the absence of stonin 2. *Proc. Natl. Acad. Sci. USA* 110, E526–E535.
- Koo, S.J., Markovic, S., Puchkov, D., Mahrenholz, C.C., Beceren-Braun, F., Maritzen, T., Dornedde, J., Volkmer, R., Oschkinat, H., and Haucke, V. (2011). SNARE motif-mediated sorting of synaptobrevin by the endocytic adaptors clathrin assembly lymphoid myeloid leukemia (CALM) and AP180 at synapses. *Proc. Natl. Acad. Sci. USA* 108, 13540–13545.
- Lampe, A., Haucke, V., Sigrist, S.J., Heilemann, M., and Schmoranzler, J. (2012). Multi-colour direct STORM with red emitting carbocyanines. *Biol. Cell* 104, 229–237.
- Liu, K.S., Siebert, M., Mertel, S., Knoche, E., Wegener, S., Wichmann, C., Matkovic, T., Muhammad, K., Depner, H., Mettke, C., et al. (2011). RIM-binding protein, a central part of the active zone, is essential for neurotransmitter release. *Science* 334, 1565–1569.
- Menon, P., Deane, R., Sagare, A., Lane, S.M., Zarcone, T.J., O'Dell, M.R., Yan, C., Zlokovic, B.V., and Berk, B.C. (2010). Impaired spine formation and learning in GPCR kinase 2 interacting protein-1 (GIT1) knockout mice. *Brain Res.* 1317, 218–226.
- Miesenböck, G., De Angelis, D.A., and Rothman, J.E. (1998). Visualizing secretion and synaptic transmission with pH-sensitive green fluorescent proteins. *Nature* 394, 192–195.
- Miśkiewicz, K., Jose, L.E., Bento-Abreu, A., Fislage, M., Taes, I., Kasprzewicz, J., Swerts, J., Sigrist, S., Versées, W., Robberecht, W., and Verstreken, P. (2011). ELP3 controls active zone morphology by acetylating the ELKS family member Bruchpilot. *Neuron* 72, 776–788.
- Mullen, G.P., Grundahl, K.M., Gu, M., Watanabe, S., Hobson, R.J., Crowell, J.A., McManus, J.R., Mathews, E.A., Jorgensen, E.M., and Rand, J.B. (2012). UNC-41/stonin functions with AP2 to recycle synaptic vesicles in *Caenorhabditis elegans*. *PLoS ONE* 7, e40095.
- Oswald, D., Fouquet, W., Schmidt, M., Wichmann, C., Mertel, S., Depner, H., Christiansen, F., Zube, C., Quentin, C., Körner, J., et al. (2010). A Syd-1 homologue regulates pre- and postsynaptic maturation in *Drosophila*. *J. Cell Biol.* 188, 565–579.
- Phillips, G.R., Huang, J.K., Wang, Y., Tanaka, H., Shapiro, L., Zhang, W., Shan, W.S., Arndt, K., Frank, M., Gordon, R.E., et al. (2001). The presynaptic particle web: ultrastructure, composition, dissolution, and reconstitution. *Neuron* 32, 63–77.
- Sakaba, T., Kononenko, N.L., Bacetic, J., Pechstein, A., Schmoranzler, J., Yao, L., Barth, H., Shupliakov, O., Kobler, O., Aktories, K., and Haucke, V. (2013). Fast neurotransmitter release regulated by the endocytic scaffold intersectin. *Proc. Natl. Acad. Sci. USA* 110, 8266–8271.
- Schikorski, T. (2014). Readily releasable vesicles recycle at the active zone of hippocampal synapses. *Proc. Natl. Acad. Sci. USA* 111, 5415–5420.
- Segura, I., Essmann, C.L., Weinges, S., and Acker-Palmer, A. (2007). Grb4 and GIT1 transduce ephrinB reverse signals modulating spine morphogenesis and synapse formation. *Nat. Neurosci.* 10, 301–310.
- Stimson, D.T., Estes, P.S., Rao, S., Krishnan, K.S., Kelly, L.E., and Ramaswami, M. (2001). *Drosophila* stoned proteins regulate the rate and fidelity of synaptic vesicle internalization. *J. Neurosci.* 21, 3034–3044.
- Verstreken, P., Ohyama, T., and Bellen, H.J. (2008). FM 1-43 labeling of synaptic vesicle pools at the *Drosophila* neuromuscular junction. *Methods Mol. Biol.* 440, 349–369.
- Watanabe, S., Rost, B.R., Camacho-Pérez, M., Davis, M.W., Söhl-Kielczynski, B., Rosenmund, C., and Jorgensen, E.M. (2013). Ultrafast endocytosis at mouse hippocampal synapses. *Nature* 504, 242–247.
- Won, H., Mah, W., Kim, E., Kim, J.W., Hahm, E.K., Kim, M.H., Cho, S., Kim, J., Jang, H., Cho, S.C., et al. (2011). GIT1 is associated with ADHD in humans and ADHD-like behaviors in mice. *Nat. Med.* 17, 566–572.
- Xu, J., Luo, F., Zhang, Z., Xue, L., Wu, X.S., Chiang, H.C., Shin, W., and Wu, L.G. (2013). SNARE proteins synaptobrevin, SNAP-25, and syntaxin are involved in rapid and slow endocytosis at synapses. *Cell Rep* 3, 1414–1421.
- Zhang, H., Webb, D.J., Asmussen, H., Niu, S., and Horwitz, A.F. (2005). A GIT1/PIX/Rac/PAK signaling module regulates spine morphogenesis and synapse formation through MLC. *J. Neurosci.* 25, 3379–3388.